Azetidinium Lead Iodide for Perovskite Solar Cells

S. R. Pering[a], W. Deng[a], J. R. Troughton[c], D. Ghosh[e], R. G. Niemann[a], F. Brivio[a], P. S. Kubiak[a,b], F. E. Jeffrey[d], A.B. Walker[e], M.S. Islam[a,d] T. M. Watson[c], P.R. Raithby[a], A.L. Johnson[a,d], S. E. Lewis[a,d], & P. J. Cameron[a,d]

[a]: Department of Chemistry, University of Bath, Claverton Down, Bath, BA2 7AY, UK
[b]: Centre for Doctoral Training in New and Sustainable Photovoltaics, University of Liverpool
[c]: SPECIFIC, Swansea University College of Engineering, Bay Campus, Swansea, SA1 8EN, UK
[d]: Centre for Sustainable Chemical Technologies, University of Bath, Claverton Down, Bath, BA2 7AY, UK
[e]: Department of Physics, University of Bath, Claverton Down, Bath, BA2 7AY, UK

Experimental

4.1. Computational calculations

4.1.1. Dipole calculations

The calculated dipoles have been obtained using the NWChem code. [39] The initial input obtained by geometrical intuition has been optimized. To express the wavefunction we used the cc-pVTZ basis set provided within the package and the as exchange correlation functional we used the B3lyp. The obtained values are in good agreement with other reports in literature. [40,41]

4.1.2. DFT calculations

Density functional theory (DFT) based calculations were performed in this study (using the CP2K code [42]). The parent tetragonal phase of $MAPbI_3$ lattice was modelled by a large 3x3x2 supercell (containing 48 A-site cations), which allowed us to simulate the small concentration of Az cations (up to 5%) The calculations employed an auxiliary plane wave basis set,[43] an energy cut-off of 350 Ry, an analytical duel-space pseudopotential as implemented by Goedecker, Teter, and Hutter (GTH),[44] and the GGA of Perdew-Burke-Ernzerhof (PBEsol).[45] Additionally, we apply van der Waals interactions, as prescribed by Grimme.[46] To obtain the ground state geometry, we relax all atoms till the interatomic forces become less than 0.02eV/Å. To calculate the substitution energy (E_{subs}), the following was been used,

$E_{subs} = (E_{MA(1-x)AzxPbI3}^{+}) - (E_{MAPbI3} + xE_{Az})$

where $E_{MA(1-x)AzxPbI3}$, E_{MAPbI3}, E_{MA} and E_{Az} were the total energies of the mixed cation lattice, parent lattice and MA^+ and Az^+ cations, respectively.

4.2. Azetidinium iodide preparation

5 ml of Azetidine (Alfa Aesar) at 0 °C had 55 mL hydroiodic acid (Sigma) added to it under argon atmosphere **(Caution! Exotherm)**. The ice bath was subsequently removed, and the solution was stirred for one hour. The solution was then left on a rotary evaporator until dry, leaving a bright orange solid. This was washed with diethyl ether to remove the iodine, and recrystallized in isopropanol, leaving white needle-like crystals. The identity of azetidinium iodide (AzI) was confirmed by ^{1}H NMR (Figure S1): (300 MHz, D_2O, δ): 2.46 (quin, J = 8.29 Hz, 2 H) δ 4.04 (t, J = 8.5 Hz, 4 H)

4.3. Crystal formation

0.1 mmol PbI_2 and AzI were dissolved in 1 mL *N*,*N*-dimethylformamide, and single crystals were grown by the solvent evaporation method.

4.4. Film deposition

For optical and structural measurements the perovskite films were deposited on to microscope glass following a method by Zheng *et al.*[35] Before film deposition, the substrates were cleaned by sonication in 2% Hellmanex solution in water, followed by deionised water, acetone and isopropanol at 90 °C. Lastly they were treated with UV/Ozone for 20 minutes. 100 µL of a 1 M solution of PbI_2 (Sigma-Aldrich) in *N*,*N*-dimethylformamide was spin-coated at 2000 rpm for 60 seconds, followed immediately by 100 µL of isopropanol spun at the same rate. The resulting PbI_2 film was dried at 60 °C for 30 minutes. Solutions containing

varying mole percentages of azetidinium iodide compared to methylammonium iodide were prepared in isopropanol, with a concentration of 20 $mgml^{-1}$. 100 µL of these solutions were pipetted onto the PbI_2 films, and spun for 60 seconds at 2000 rpm. The perovskite films were annealed at 100 °C for 20 minutes.

4.5. Solar cell fabrication

Pre-etched FTO glass (Kintek) was cleaned in 2% Hellmanex solution in water, followed by deionised water, acetone and isopropanol. A compact TiO_2 layer was deposited by spray pyrolysis. A hand held atomiser was used to spray a solution of 10 vol% solution of titanium isopropoxide (bisacetylacetonate) (Sigma-Aldrich) in isopropanol onto the substrates, which were kept at 550 °C for the procedure, and sintered for 30 minutes at the same temperature. A mesoporous layer consisting of a 2:7 mixture of 30 NR-D TiO_2 paste (Dyesol) in ethanol was spun onto the compact layer with a further 30 minute sintering step at 550 °C. After cooling, to improve conductivity a 0.1 M solution of Li-TFSI (Sigma) solution was spin-coated at 3000 rpm for 10 seconds and the substrates were then re-sintered at 550 °C for 30 minutes. Perovskite deposition was performed in a nitrogen filled glove box. A two-step dip-coating method was used to fabricate the solar cells. 1M PbI_2 in DMF was kept at 70 °C for spin-coating. 100 µL of PbI_2 solution was spin-coated at 6500 rpm for 30s, then dried at 100 °C for 30 minutes. A 5 minute dipping step in the MAI or mixed MAI/AzI in IPA solution (10 $mgml^{-1}$, AzI fractions in mol% with respect to MAI). The films were annealed at 100 °C for 1 hour.

The hole transport layer solution consisted of 85 $mgml^{-1}$ Spiro-OMeTAD (Ossila) in chlorobenzene, with additives of: 30 μLml^{-1} *t*-butyl pyridine (Sigma), 20 μLml^{-1} of 520 $mgmL^{-1}$ Li-TFSI in acetonitrile and 30 μgmL^{-1} FK209-TFSI solution. This was spin-coated onto the perovskite at 4000 rpm for 30 seconds.

To establish the contacts, 2 mm of perovskite was removed from the centre of the substrate. 100 nm of gold (Kurt J Lesker) was deposited by thermal evaporation.

4.6. SCXRD, PXRD

Crystal X-ray diffraction was performed on an Agilent Technologies EOS S2 Supernova, using a Cu X-ray source.

A Bruker axs D8 advance powder x-ray diffractometer with a Cu Kα source and Ge monochromator was used for Powder X-ray diffraction. Measurements were taken from 2θ values of 5 ° to 80 °.

4.7. UV/vis spectroscopy

Thin film optical Transmission and Reflectance measurements were performed on a Perkin-Elmer Lambda 750S UV/Vis spectrometer, from 1000 nm to 250 nm. Absorption was calculated as incident light– (transmission + reflectance).

4.8. Raman spectroscopy

Raman measurements were performed with a Renishaw in via Reflex microRaman spectrometer equipped with solid state lasers emitting at 514 and 785 nm with a resolution of $< 2\ cm^{-1}$. The laser beam was focused with a x50 magnification lens, giving a laser spot size of about 1 μm in diameter. Rayleigh scattering was rejected with a 110 cm−1 cutoff dielectric edge filter. The AzI sample was measured with a 514 nm laser and the orange AzPI with the 785 nm laser in order to avoid resonant effects in the sample. All measurements were performed in air and with different laser powers to ensure that the laser probe did not induce damage or changes in the sample

4.9. Electrochemical measurements

An Autolab potentiostat/galvanostat was used for solution based electrochemistry, using an Ag/AgCl reference electrode and a platinum counter electrode. 0.1 mol azetidinium iodide in

isopropanol was used as the electrolyte. For Mott-Schottky measurements the frequency was 27 Hz and the voltage was swept stepwise from -0.1 to 0.75 V vs Ag/AgCl.

4.10. J-V curves

J-V curves were measured using a Keithley 2601A potentiostat, under 1 Sun intensity and at AM 1.5. The cell was sweeped at 100 mVs^{-1} from 1.1 V to -0.1 V and back to 1.1 V. The 8 pixels with a 0.1 cm^2 active area (obtained using a mask) were measured independently.

A Newport Oriel 91150-KG5 reference cell with a KG5 filter was used for instrument calibration.

EQE measurements were taken in 10 nm steps from 380-850 nm.

4.11. Scanning Electron Microscopy

SEM images were taken on a JEOL SEM 6480LV, at an acceleration voltage of 10kV.

4.12 Atomic Force Microscopy

AFM images were taken on a Nanosurf easyscan 2 FlexAFM system in dynamic mode using a force of 20 nN. A ContAl-G Tip was used for measurements

Supporting Information

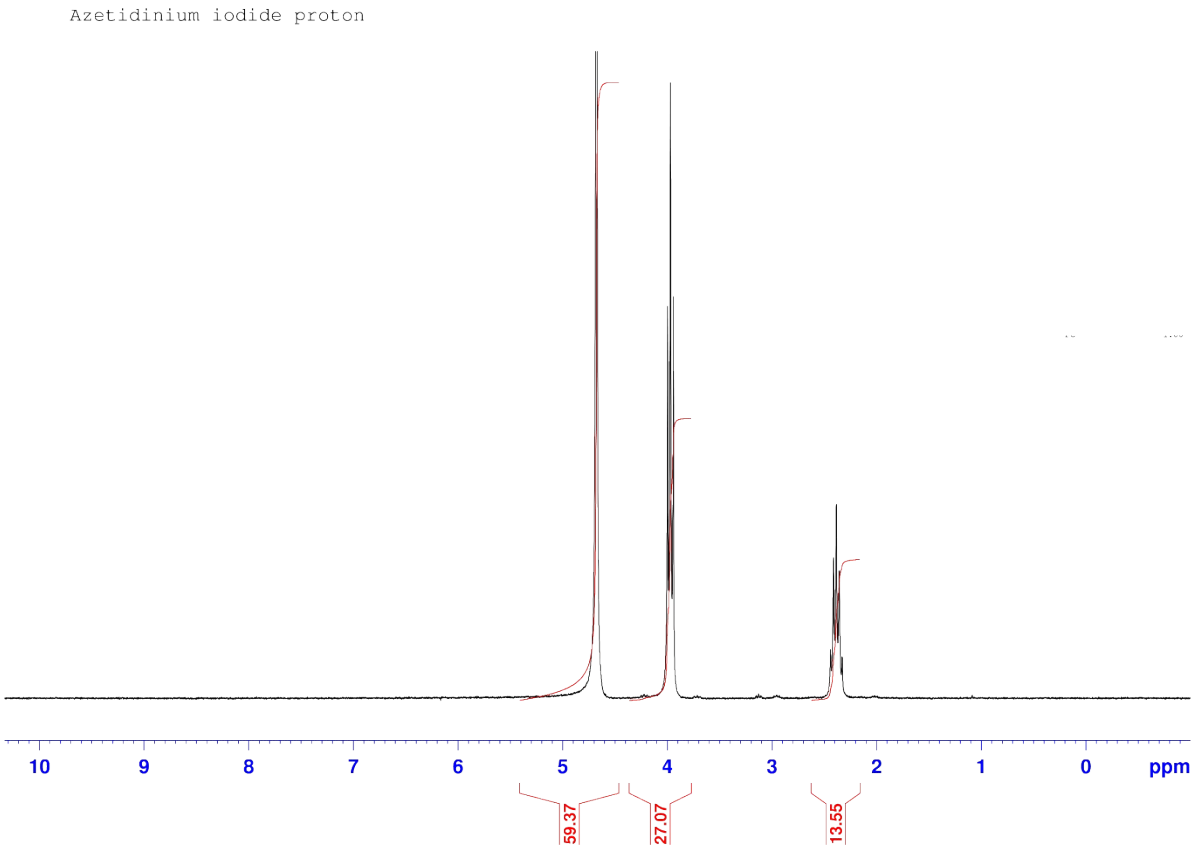

Figure S1: Azetidinium Iodide ^{1}H NMR Spectrum (Taken in D_2O on a 300 MHz Spectrometer)

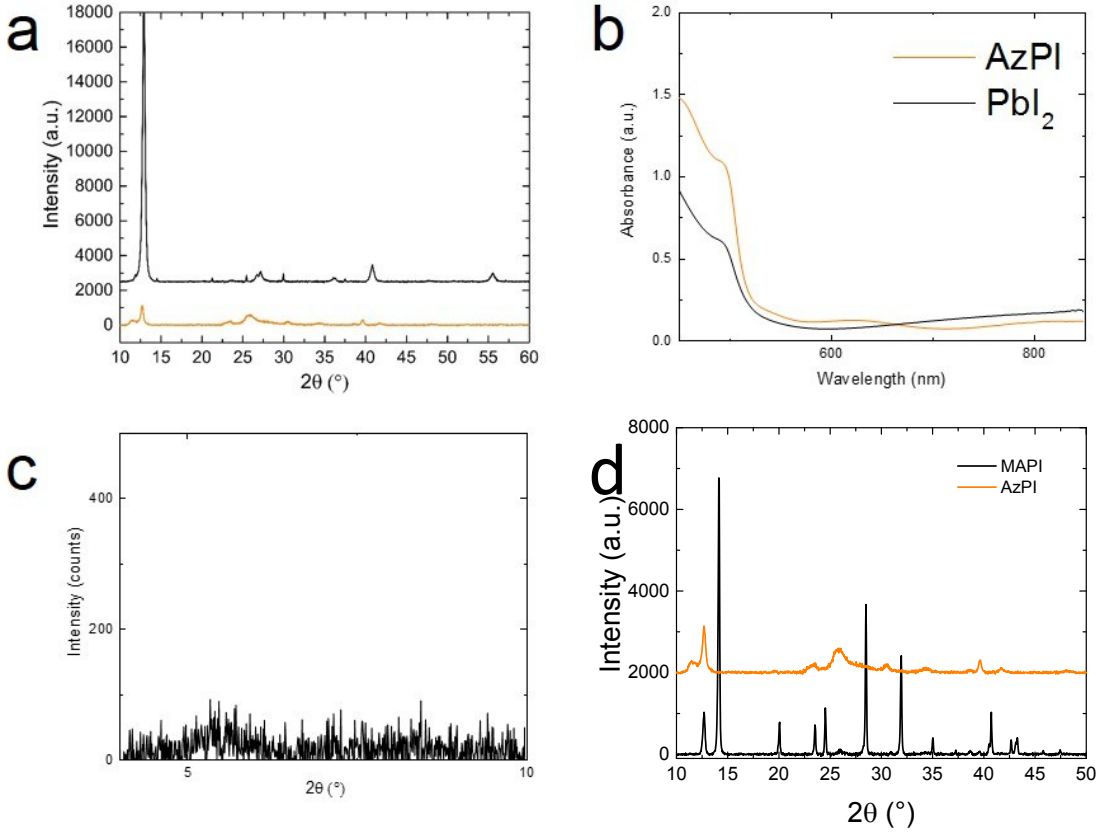

Figure S2: A comparison of AzPI to PbI_2 and MAPI (a) XRD of PbI_2 (black) and AzPI (orange), (b) UV/Vis of PbI_2 (black) and AzPI (orange) (c) low angle XRD of AzPI, and (d) MAPI (black) and AzPI (orange) XRD plots

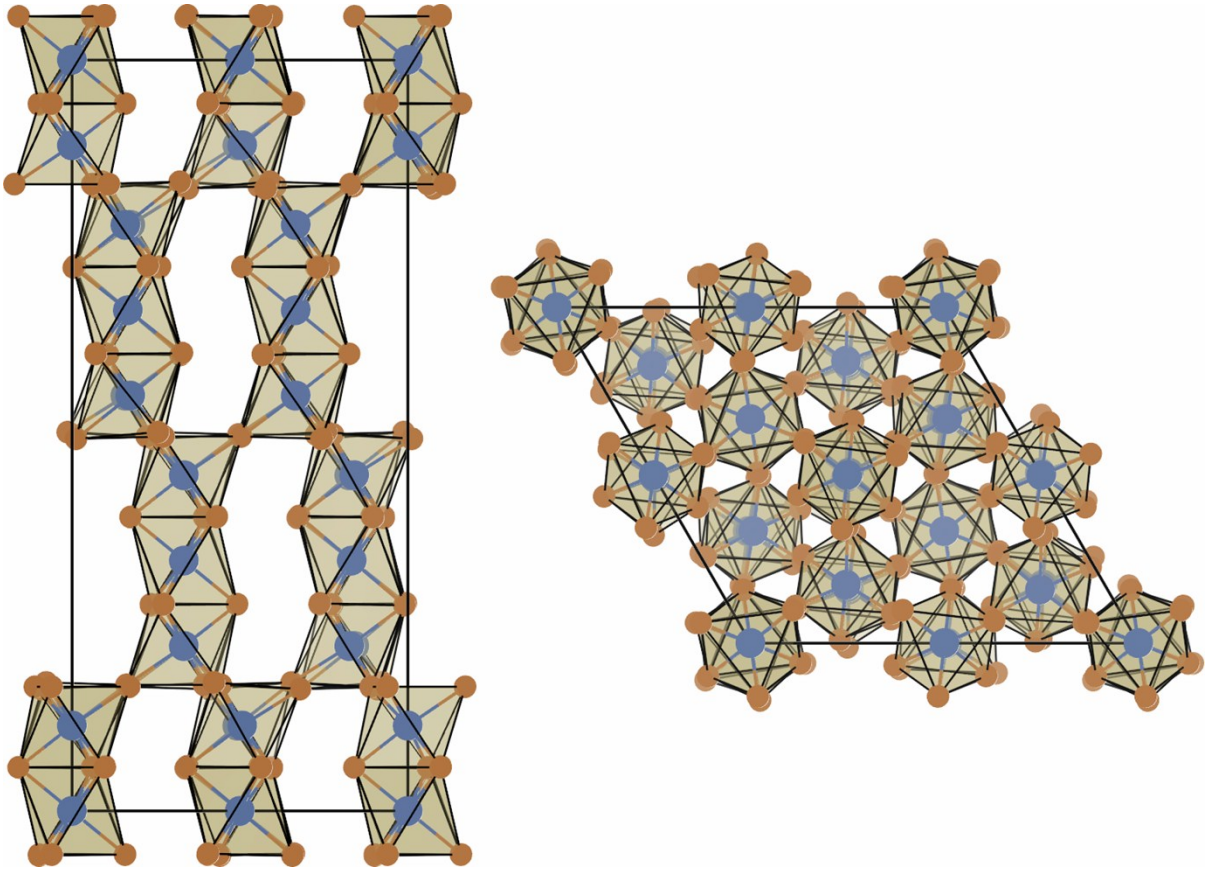

Figure S3: PbI_2 skeleton suggested by SCXRD – it should be stressed that the degree of twinning was severe.

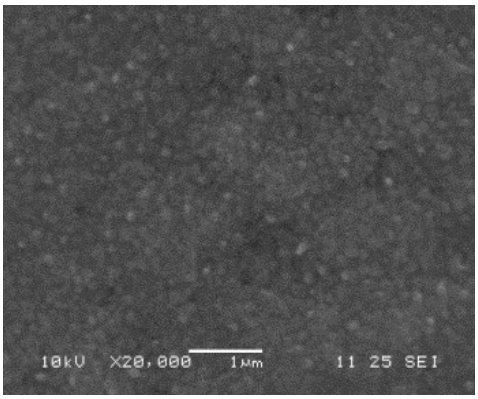

Figure S4: SEM image of an AzPI film

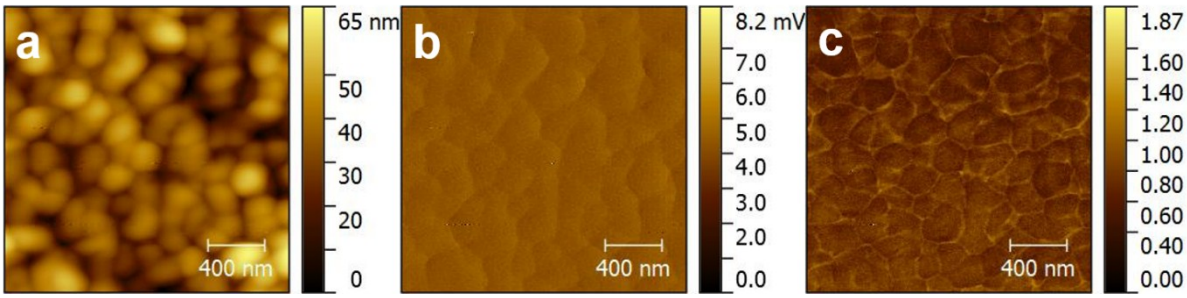

Figure S5 AFM Images of an AzPI film: (a) z-axis, (b) amplitude and (c) phase

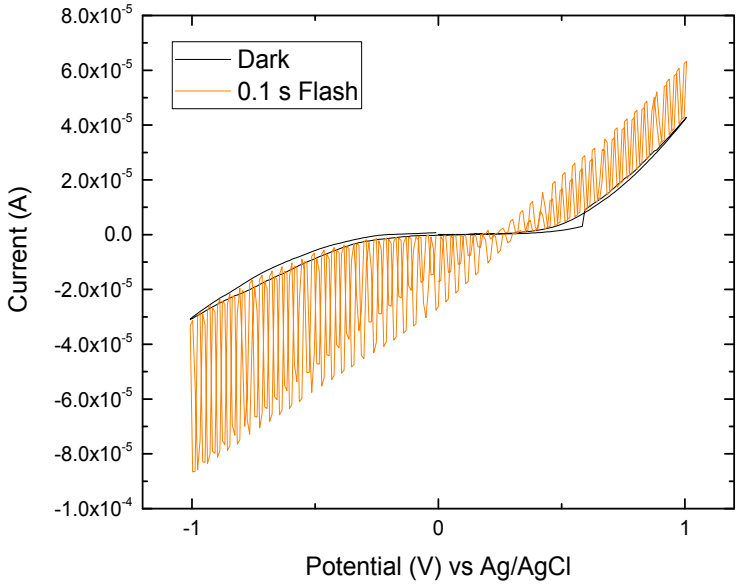

Figure S6: Chopped photocurrent measurement of AzPI on FTO, in 0.1 M AzI in IPA electrolyte, with Pt counter electrode and Ag/AgCl reference.

Table S1. Comparison of all measured Raman modes of $AzPbI_3$, AzI and Az with provisional peak assignment.

Az (DFT)	AzI	rel. shift	AzPI	Assignment	
361				ν_1	Ring pucker
			693	ν_2	N-H bend (in plane)
808	785	↓ 15	770	ν_3	Ring deform
	883	↓ 8	875	ν_4	2-CH_2 twist
	911	↓ 12	899	ν_5	2-CH_2 rock
961	956	↓ 5	951	ν_6	1-CH_2 rock
1009	1012	↓ 4	1008	ν_7	2-CH_2 rock
	1217			ν_8	1-CH_2 wag
1254	1245	↑ 7	1252	ν_9	1-CH_2 twist
1313	1283	↓ 6	1277	ν_{10}	2-CH_2 twist
1385	1302			ν_{11}	1-CH_2 twist
1452	1455			ν_{12}	1-CH_2 wag
1534	1511	↓ 61	1450	ν_{13}	NH_2 wag
1655	1582			ν_{14}	2-CH_2 scissor
2982	2980	↓ 8	2972	ν_{15}	1-C-H stretch
3020	3019			ν_{16}	2-C-H-stretch

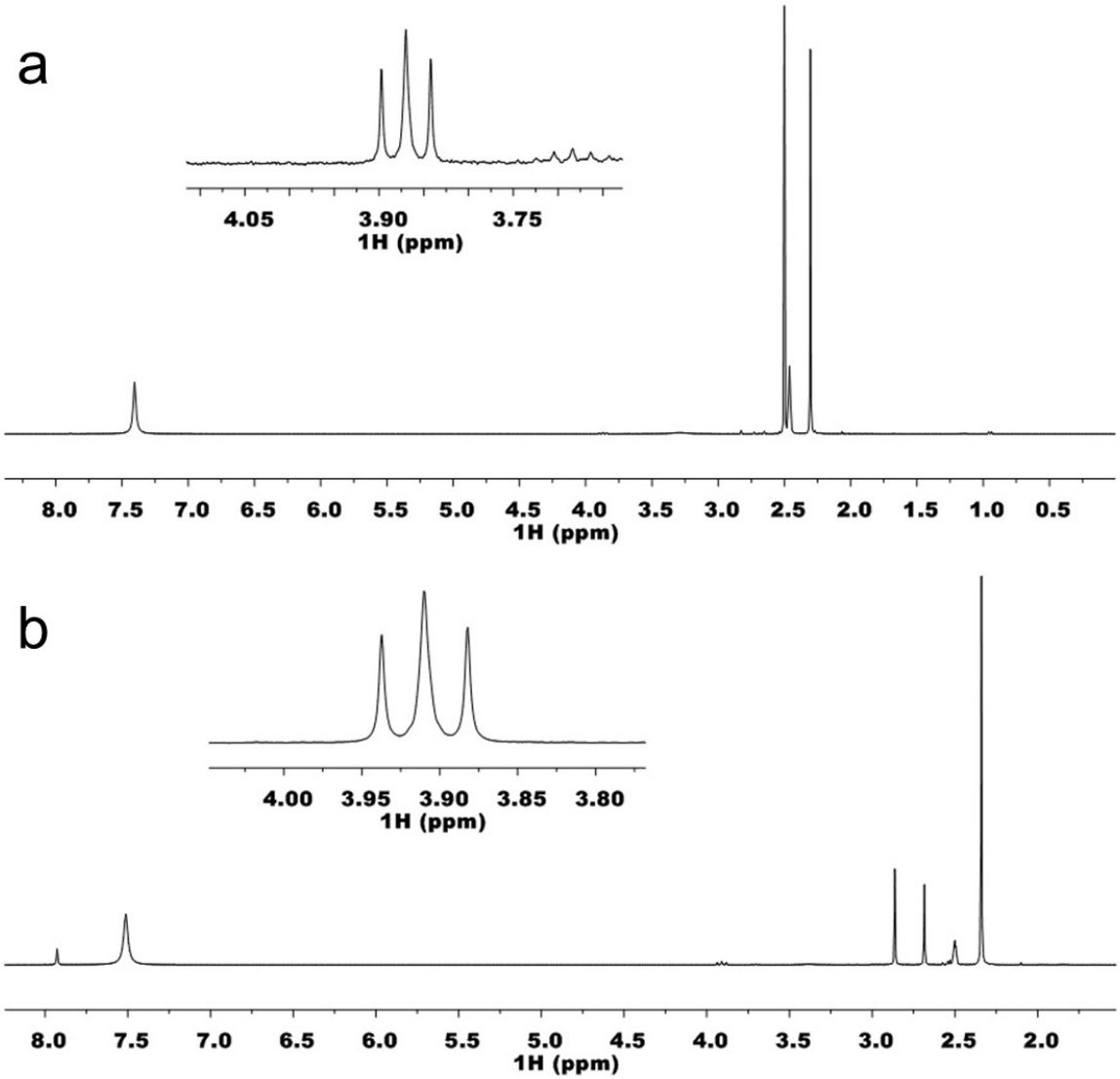

Figure S7: ^{1}H NMR Spectrum (Taken in DMSO-d6 on a 300 MHz Spectrometer) for: a) 1 mol% AzMAPI, and b) 5 mol%, both with the Azetidinium peak at δ 3.9 inset.

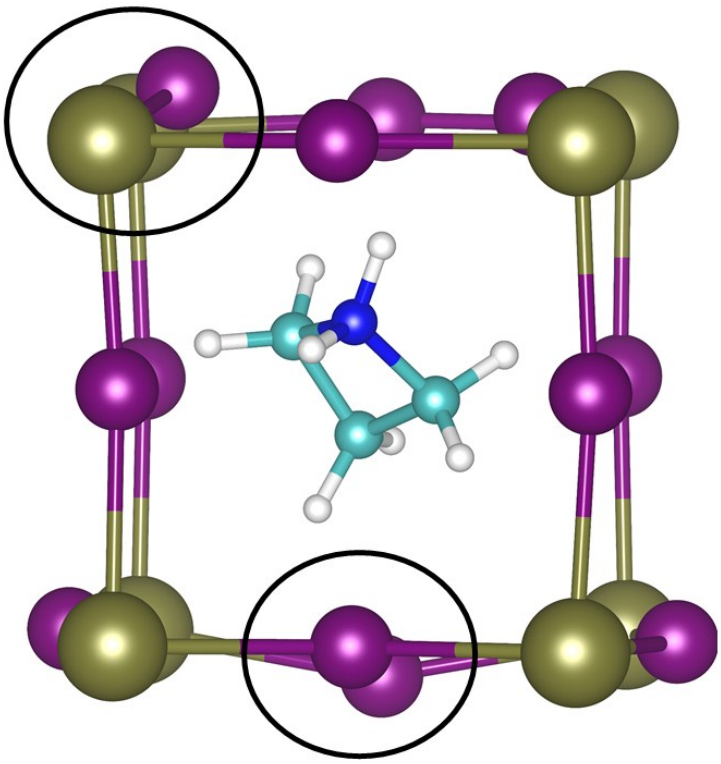

Fig S8. The optimized geometry of Pb/I lattices near to Az^+ cations. The local lattice distortion of Pb/I frame due to presence of Az^+ cation can be evidently seen and further marked by the black circles.

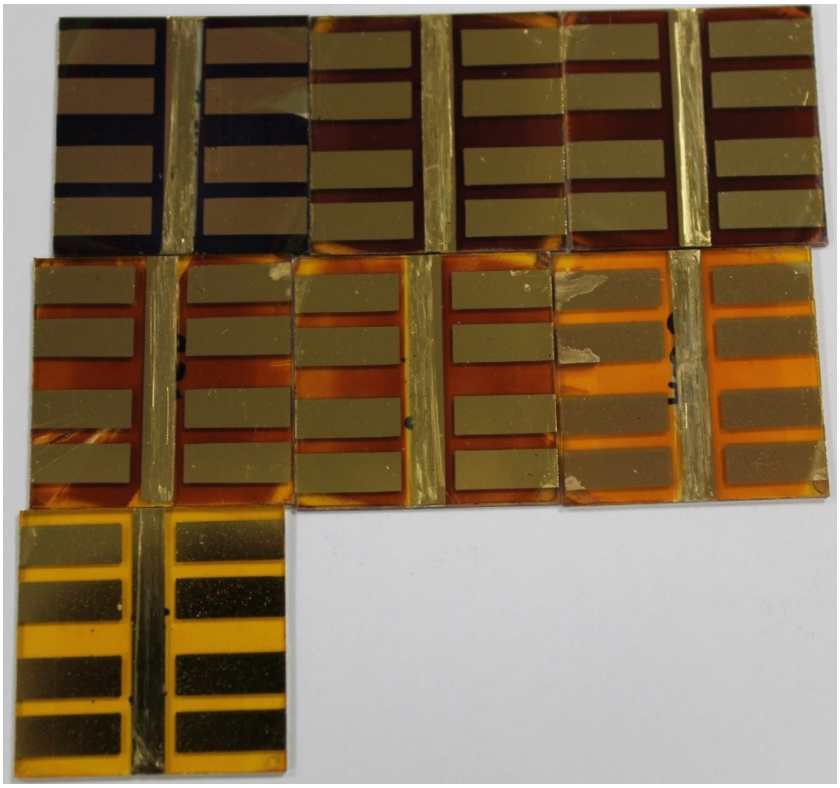

Fig. S9: A photograph of the MAPI/AzMAPI solar cell, from left to right: (top) MAPI, A1, A2 (middle) A5, A10, A25 (bottom), AzPI

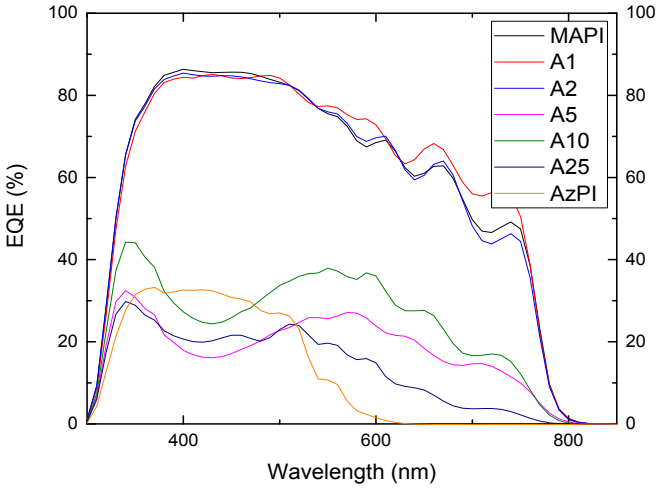

Fig. S10: EQE measurements for the best performing pixels for each mixture of MAPI, AzMAPI or AzPI

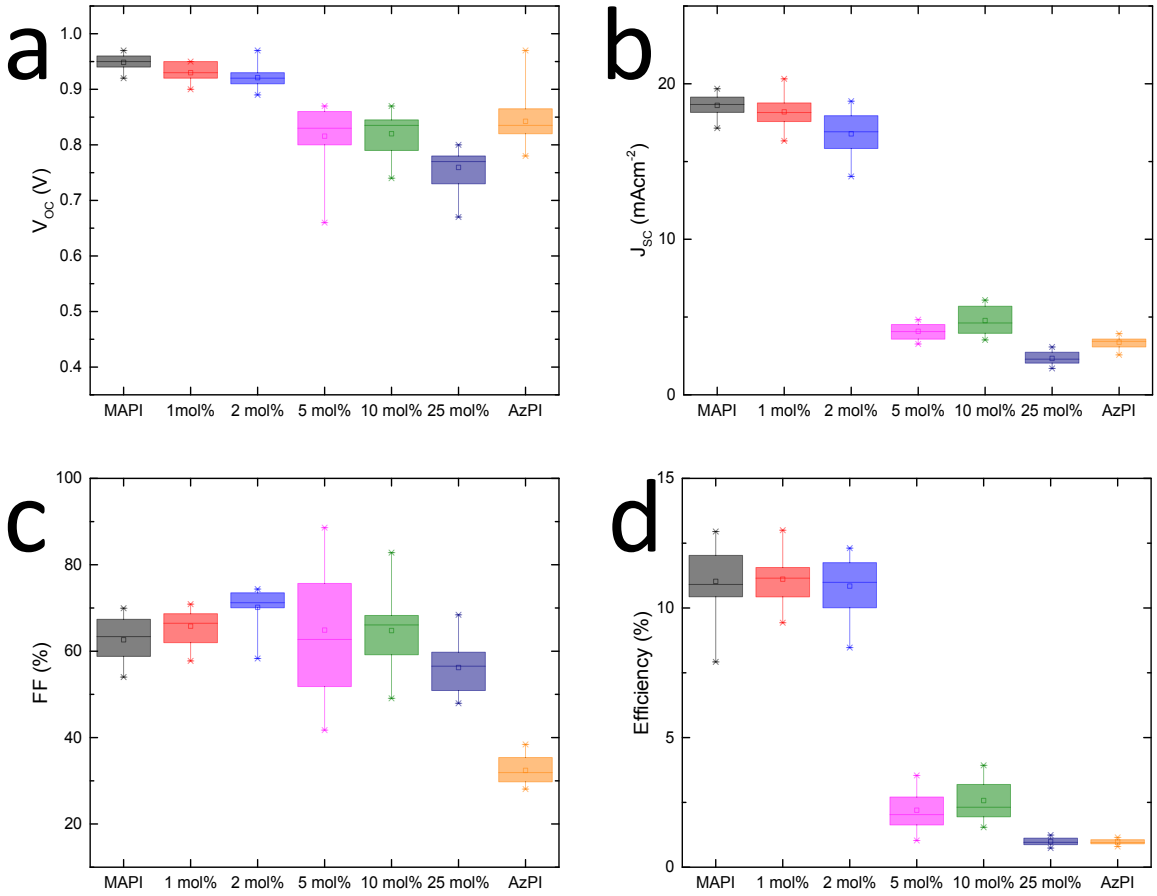

Fig. S11 Box plots for the cell parameters of AzMAPI cells: (a) V_{OC} (b) J_{SC} (c) Fill Factor and (d) Efficiency

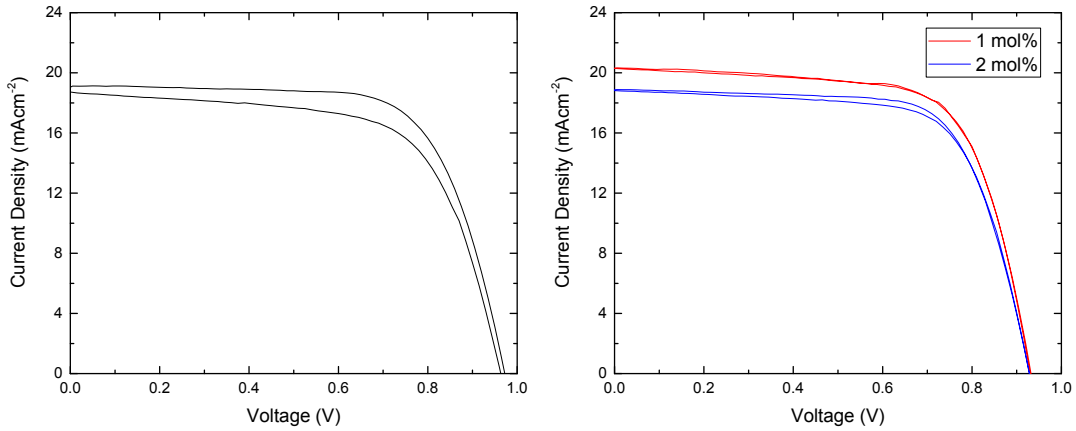

Figure S12. A comparison of the hysteresis in the JV curves for MAPI cells (left) and those with azetidinium additives

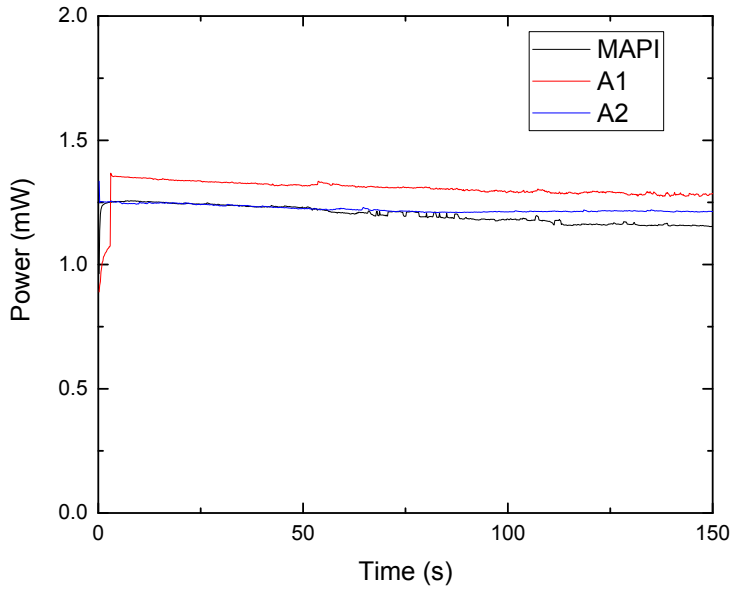

Figure S13. Stabilised power output measurements for the best performing AzMAPI and MAPI pixels

References:

39 M. Valiev, E.J. Bylaska, N. Govind, K. Kowalski, T.P. Straatsma, H.J.J. Van Dam, D. Wang, J. Nieplocha, E. Apra, T.L. Windus, W.A. De Jong *Comput. Phys. Commun.* 2010, **181** (9), 1477–1489.

40 J. Frost, K. Butler, F. Brivio, *Nano Lett.* 2014, **14** (5), 2584–2590

41 F. Zheng, H. Takenaka, F. Wang, N.Z. Koocher, A.M. Rappe *J. Phys. Chem. Lett.* 2015, **6** (23), 31–37.

42 J. Hutter, M. Iannuzzi, F. Schiffmann and J. VandeVondele, *Wiley Interdisciplinary Reviews: Computational Molecular Science*, 2014, **4**, 15–25

43 J. VandeVondele, M. Krack, F. Mohamed, M. Parrinello, T. Chassaing and J. Hutter, *Comput. Phys. Commun*., 2005,**167**, 103–128.

44 S. Goedecker, M. Teter and J. Hutter, *Phys. Rev. B*, 1996, **54**,1703.

45 J.P. Perdew, A. Ruzsinszky, G. I. Csonka, O. A. Vydrov, G. E. Scuseria, L. A. Constantin, X. Zhou, and K. Burke, *Phys. Rev. Lett*. 2009, **100,** 136406

46 S. Grimme, *J. Comput. Chem*, 2006, **27**, 1787–1799